IEEE Access
Multidisciplinary | Rapid Review | Open Access Journal

Received March 25, 2020, accepted March 31, 2020, date of publication April 2, 2020, date of current version April 17, 2020.

Digital Object Identifier 10.1109/ACCESS.2020.2985216

Pavement Crack Detection Using Progressive Curvilinear Structure Anisotropy Filtering and Adaptive Graph-Cuts

ZHENHUA LI[1], GUILI XU[1,2], YUEHUA CHENG[1], ZHENGSHENG WANG[3], AND QUAN WU[1]

[1]College of Automation Engineering, Nanjing University of Aeronautics and Astronautics, Nanjing 211106, China
[2]Nondestructive Detection and Monitoring Technology for High Speed Transportation Facilities, Key Laboratory of Ministry of Industry and Information Technology, Nanjing 211106, China
[3]College of Science, Nanjing University of Aeronautics and Astronautics, Nanjing 211106, China

Corresponding author: Guili Xu (guilixu@nuaa.edu.cn)

This work was supported in part by the National Natural Science Foundation of China under Grant 61473148, and in part by the National Key Research and Development Plan under Grant 2016YFB0500803.

ABSTRACT Delineation of pavement cracks is essential for the damage assessment and maintenance of pavements. Existing methods are not sufficiently robust to interferences including varied illumination, non-uniform intensity, and complex texture noise. An integrated system for the automatic extraction of pavement cracks based on progressive curvilinear structure filtering and optimized segmentation techniques is proposed in this paper. Considering phase congruency and path morphological transformation, a phase congruency guided multi-scale path anisotropy filtering (PCmPA) method is first developed to generate a crack saliency map, significantly enhancing crack structures and eliminating isotropic texture noise. Phase congruency guided multi-scale free-form anisotropic filter (PCmFFA) is then presented as an extended curvilinear structure filter considering context information to enhance PCmPA. Finally, to accurately identify crack pixels and background, the two independent global filtering responses are incorporated with the phase congruency map and integrated into the graph-cuts based global optimization model with an adaptive regularization parameter. Experiments are conducted on two public pavement datasets and a self-captured laser-scanned pavement dataset, with results demonstrating that the proposed method can achieve superior performance compared to six existing algorithms.

INDEX TERMS Crack detection, curvilinear structure filtering, phase congruency, optimized segmentation, graph-cuts.

I. INTRODUCTION

The demand for reliable automated pavement crack detection techniques has risen significantly with increasing use of intelligent pavement distress inspection. Cracks are common and harmful road surface defects that directly affects road service-life and driving safety. Detection of them early can provide a reliable decision-making basis for efficient management and maintenance of structured road networks, which is of great significance in reducing the economic burden induced by subsequent deterioration and eliminating safety hazards. In the past decades, intelligent pavement crack detection techniques are drawing increasing attention because of its essential for the health monitoring and assessment of civil infrastructures [1]–[4]. These techniques incorporate concepts from other curvilinear object detection tasks including vessel segmentation [5], cartographic extraction [6], road network extraction [7], and guide-wire tracking [8]. Despite a large field of application and decades of extensive research, the gap between current state-of-the-art methods and performance goals remains large.

Factors that create challenges to the task of automated pavement crack detection predominantly include uncertain interferences such as uneven illumination, varied appearance of crack structures, and unpredictable isotropic structures such as blob-like or plane-like clutter. Reasonable excavation and utilization of the gray distribution and geometric structure characteristics of pavement cracks can provide an effective way to solve this problem. For example, local-based methods including second-order derivatives of Gaussian kernel

The associate editor coordinating the review of this manuscript and approving it for publication was L. Zhang.

based method [9], [10], diffusion tensors [11], steerable filter [12]–[14], and wavelet based filters [15], utilize local analyses of intensity and orientation to detect cracks based on the assumption that cracks are generally darker than their surroundings and with obvious line-like structure. While such methods are simple and intuitive, they are also highly sensitive to textured noise and have low discriminative power for complex pavement images. Conversely, non-local approaches, such as path-based methods [16]–[18], traditional machine learning based methods [2], [19]–[26], and deep learning based techniques [1], [3], [4], [27], focus more on global hypotheses, characterizing curvilinear structures in larger neighborhoods, and can achieve significantly improved performance compared to local-based approaches in textured occasions. While path-based methods dramatically improve the identification ability of line-like and interference targets, drawbacks include low contrast between detected curvilinear structures and background and weak continuity of the detected target. Benefitting from a large amount of precisely labeled datasets, deep learning-based methods such as the work [27] and DeepCrack [3], can achieve highly accurate crack detection, however, it is difficult to directly transform the trained models to other application scenarios.

Although current research methods have achieved certain results, automatic pavement crack detection in noisy backgrounds remains challenging for the following reasons: (1) Current methods can easily succumb to interference from complex backgrounds and have poor robustness to illumination variation and intensity non-uniformity; (2) Most current methods model the local geometric properties of ideal line-like cracks, so complex geometry with sharp bends and discontinuity may not be appropriately identified; (3) For the final process of determining of pixel-level cracks, cumbersome post-processing operations are required.

An integrated system for the automatic extraction of crack networks from 2D textured pavement images is proposed in this paper to address these issues. The proposed algorithm pipeline is illustrated in Fig. 1. Phase congruency tuned at varying orientation and scales are first used to enhance edge-like structures. To effectively discriminate isotropic and curvilinear structures, the progressive multi-scale anisotropy features PCmPA and PCmFFA are then extracted from phase congruency map to consider the local contextual information of crack structures. Finally, a novel graph-cuts based optimized segmentation model with adaptive regularization parameter is utilized to further obtain pixel-wise crack networks.

The contributions of this paper can be summarized as follows:

- Two types of multi-scale anisotropic filtering approaches, PCmPA and PCmFFA, that can be applied to pavement images with complex background interference are proposed.
- Combining appearance feature and geometric prior knowledge extracted by the proposed filters, a novel graph-cuts based optimized segmentation model is designed to promote the classification of crack pixels. In addition, an adaptive regularization parameter determined method is presented for the model.
- Experiments are conducted using both public pavement datasets and the authors' self-captured laser scanning images, and the experimental results demonstrate the effectiveness of the proposed method.

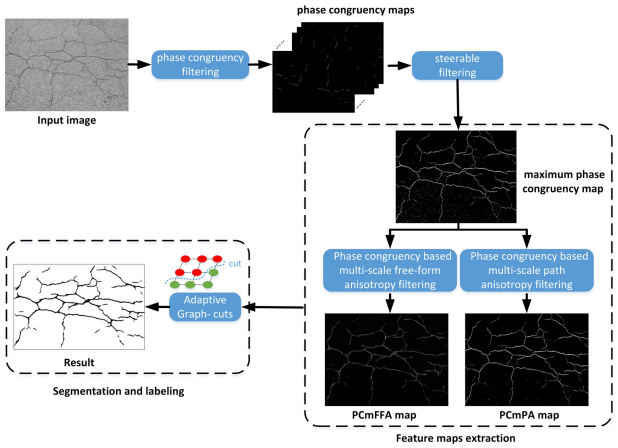

FIGURE 1. Framework of the proposed approach.

The remainder of this paper is organized as follows: Related work is discussed in Section II. Section III presents the two anisotropy filters and explains the optimized segmentation model in detail. Section IV describes the experimental results on a series of pavement crack datasets and evaluates the proposed algorithm. Finally, Section V concludes the paper.

II. RELATED WORK

Recent years have witnessed noteworthy progress in pavement cracks detection. In terms of the mathematical tools being utilized, these approaches can be divided into several categories.

Early works are primarily aimed at detecting cracks by employing their intensity or local geometric features, assuming that cracks exhibit line-like structure in a local range and differ morphologically from the non-crack regions. Filter-based algorithms are representative of this category. For example, by considering the local contrast and orientation characteristics, the matched filter was employed by Sollazzo *et al.* [10] to match with the specific features of crack patterns. In this process, the Gaussian curve was utilized to approximate the cross profile along cracks and a set of matched filter kernels was generated by this specific pattern. Zalama *et al.* [15] employed Gabor filters and a statistical learning system trained from a large database to detect longitudinal and transverse cracks. Li *et al.* [28] proposed a novel multi-scale curvilinear structure filter for crack contours enhancement, in which the curved-support bivariate Gaussian model was adopted to relax shape assumptions and conquer the problems of scale and curvature variant simultaneously.

To promote the robustness to texture noise, two brain-inspired trainable filters, B-COSFIRE [29] and RUSTICO [30], were proposed by Strisciuglio *et al.* and achieved favorable performance in crack detection. As most of these filter-based algorithms are built by modeling the local geometric properties of ideal crack structures, they may not appropriately identify complex cracks with sharp bends, poor continuity and bifurcations.

Mathematical morphology is another commonly used technique that models the profile of curvilinear structures as elongated patterns. In the work of Wu *et al.* [31], grayscale bottom-hat and top-hat operations composed of four-directional line-shape structuring elements were utilized to extract pixels that belong to black crack and white crack, respectively. To solve the problem of connecting and grouping crack fragments, dilation and thinning transformation have also been adopted. Different from classical opening operators that use fixed line-shape structuring elements, the path opening and closing operations [32], as originally introduced by Heijmans, are more flexible in discriminating curvilinear structures with arbitrary shapes. As they do not need to impose any constraint on the geometric characteristics of curvilinear structures, great attention has been received [16], [17], [33]. For example, in the literature [18], the original path opening model was extended by ranking the orientation responses of path operators, called RORPO, to reduce the intensity of isotropic interference objects and preserve perceptually connected curvilinear structures. However, when the crack contours become inconspicuous, the automatic implementation of these methods can be unreliable due to difficulties in designing appropriate structuring elements.

Minimal path-based approaches generally treat the crack path detection problem as determining minimum cost paths between candidate crack points and have drawn extensive attention due to their superiority in obtaining continuous crack paths. For example, in [34], the Free-Form Anisotropy (FFA) algorithm was utilized to determine the probability of each pixel belonging to crack by extracting features from four minimal paths that have been tracked along with four predefined templates. Li *et al.* proposed the FoSA approach [35], which first searches minimal paths in each candidate image block by F* algorithm and then utilize two-step post-processing contains path connection and purification to refine crack networks. To release geometric restriction on the cracks and avoid false detections, Amhaz *et al.* presented a two-stage minimal path selection algorithm, namely MPS [36], in which the endpoints within each sub-image are first selected and the minimal path between each pair of adjacent points are then searched by Dijkstra algorithm. Recently, Wissam *et al.* proposed the OMPS [37] method for the improvement of the original MPS method by optimizing candidate endpoints selection and shortest path search strategies. Although crack contours obtained by these methods exhibit good connectivity, it is difficult to design versatile seed points selection and non-crack paths removal strategies in practical applications due to changeable background texture.

Machine learning techniques play a pivotal role in crack detection. Such techniques generally rely on hand-crafted low-level features or high-level semantic information extracted from each image block to construct recognition models. In [19], the detection of bridge cracks was studied by using a modified active contour model and greedy search-based support vector machine. In CrackForest [2], structured forests [38] technique was utilized to learn crack tokens for the generation of crack detector. With the development of the computing capabilities and convenience of mass dataset acquisition, deep learning-based crack detection methods are being comprehensively developed. For example, in literature [1], deep convolutional neural networks (ConvNets) [39] were introduced to automatically learn features for low contrast pavement patches classification. Recently, an automatic crack detector based on end-to-end trainable deep convolutional neural network, namely DeepCrack [3], was investigated. Although machine learning methods are suitable for crack images with complex interference, cumbersome dataset labeling processes are required, and their performances are greatly limited by the training dataset.

III. METHODOLOGY

In this section, the generation of the proposed non-local curvilinear structure filters is explained, including phase congruency based multi-scale path anisotropy filter and the modified multi-scale free-form anisotropy filter. Implementation of the optimized segmentation model for crack pixels classification is then discussed.

A. PHASE CONGRUENCY MAPS GENERATION

Phased congruency is based on the concept that salient patterns have similar local phase value when observed at different scales. Specifically, for a curvilinear structure in an image, phase information is locally congruent, and the degree of this congruency can serve as a curvilinear detector. For a 2D image, these local phase features can be defined and extracted using a set of 2D quadrature filter pairs.

Compared to other quadrature filters, log-Gabor filters have superior capabilities for encoding natural images. In this paper, a number of 2D log-Gabor filters tuned at six different scales $\{s\}$ and 12 different orientations $\{\theta\}$ that linearly varying from $\theta \in [0, \pi]$ are employed to obtain a set of phase congruency maps. Specifically, in each specified direction θ_i, multi-scale 2D log-Gabor filtering is used to capture image phase information at different scales for the calculation of one phase consistency map PC_{θ_i} in that direction. Therefore, a total of 12 phase congruency maps $\{PC_{\theta_i} :| \ i = 1 \sim 12\}$ are generated. The higher the response of a point in map PC_{θ_i}, the more likely that a line-like pattern aligning to direction θ_i will exist and vice versa. Further information regarding the calculation and reasonably selecting relative parameters of phase congruency can be obtained from the reference [40].

B. PHASE CONGRUENCY GUIDED MULTI-SCALE PATH ANISOTROPY FILTERING

Phase congruency reveals the feature phases of an image in the frequency domain, which is an intensity and contrast independent feature metric in which curvilinear structures with low contrast can be enhanced [41]. Path morphology, as a non-local anisotropy measurement method, has demonstrated more robust capabilities for distinguishing curvilinear structures from texture noised images compared to traditional local-based approaches. Combining the strengths of these two approaches, in this subsection, a phase consistency based multi-scale anisotropy filtering (PCmPA) method is proposed to address the problem of enhancing cracks from textured images with varying illumination and contrast.

As observed, for crack targets, the distribution of phase congruency amplitude along and perpendicular to the crack direction are different. However, in background regions, the distribution along any direction path is similar. Based on this fact, crack targets can be distinguished from backgrounds by considering the distribution of phase congruency over different directions. The PCmPA is presented here by considering four orientational path opening operators to reliably discriminate curvilinear structures and isotropic structures.

First, given a phase congruency map PC_{θ_i}, where $\theta_i \in [0, \pi]$, a 2D-oriented Gaussian kernel-based steerable filter with the specified direction θ_i is adopted to amplify correlated responses and smooth out uncorrelated responses. More importantly, the filter is able to connect small gaps in phase congruency maps caused by texture noise. The enhancing process is described by Eq.(1) as follows:

$$PC^*_{\theta_i}(x, y) = PC_{\theta_i}(x, y) * G_{\theta_i}(x, y), \tag{1}$$

$$G_{\theta_i}(x, y) = e^{-\pi(\frac{xcos\theta_i + ysin\theta_i}{\sigma^2} + \frac{-xsin\theta_i + ycos\theta_i}{(\rho\sigma)^2})} \tag{2}$$

where G_{θ_i} is the oriented Gaussian kernel and σ is the variances of Gaussian distribution. The parameter $\rho \in [0.01, 1]$ is used to control the form of the Gaussian kernel so that a value close to 1 will produce a symmetric kernel, while a smaller value close to the lower bound will produce an elongated kernel. In the experiments, σ is set as 2, and ρ is set as 0.25. Each enhanced image after local convolution is denoted as $PC^*_{\theta_i}$.

Using maximum aggregation, the filtered phase congruency maps $\{PC^*_{\theta_i} :| \ i = 1 \sim 12\}$ are then grouped into one maximum phase congruency map defined as:

$$I^{max}_{PC} = \max_{\theta_i \in [0,\pi]} \left\{PC^*_{\theta_i}\right\}. \tag{3}$$

For the map I^{max}_{PC}, path opening operators with path length l under four different directional adjacency graphs $(o_j)_{j\in[1,4]}$ (shown in Fig. 2) are focused on it to count the length of a path at each pixel (x, y), and the resulting images are denoted as:

$$A^{o_j}_l(x, y) = po\left\{I^{max}_{PC}(x, y)\right\}_{o_j}. \tag{4}$$

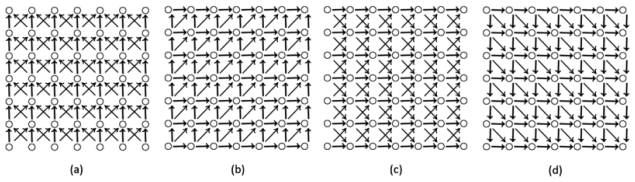

FIGURE 2. The four adjacency graphs used for the path opening algorithm. Graph (a) shows the S-N adjacency graph, graph (b) shows the SW-NE graph, (c) is the W-E adjacency graph, and (d) is the NW-SE adjacency graph.

where $po\{\cdot\}_{o_j}$ refers to the path opening operator under adjacency graph o_j.

As $A^{o_j}_l$ only represents the maximum path length that traverses each point (x, y) along orientation o_j, to estimate the probability that any point belongs to the curvilinear structure under scale l, the path anisotropy measurement is defined as:

$$PA_l(x, y) = \frac{\sqrt{(\max(A^{o_j}_l(x, y)) - \min(A^{o_j}_l(x, y)))^2}}{\max(A^{o_j}_l(x, y))^2 + \min(A^{o_j}_l(x, y))^2}. \tag{5}$$

The concept behind this metric is that for backgrounds or grain-like interferences, the values after four directional path opening operations are similar, meaning that $PA_l(x, y)$ will approach 0. A large difference remains between the operations along curvilinear structures and operations along the remaining direction, which will make $PA_l(x, y)$ approximate to 1. To preserve the anti-extensivity of the above path opening, a minimum operator is applied between the path anisotropy measurement and normalized maximal phase congruency map I^{max}_{PC}. The normalized path anisotropy measurement is then defined as:

$$PA^*_l(x, y) = \min\left\{PA_l(x, y), I^{max}_{PC}(x, y)\right\}. \tag{6}$$

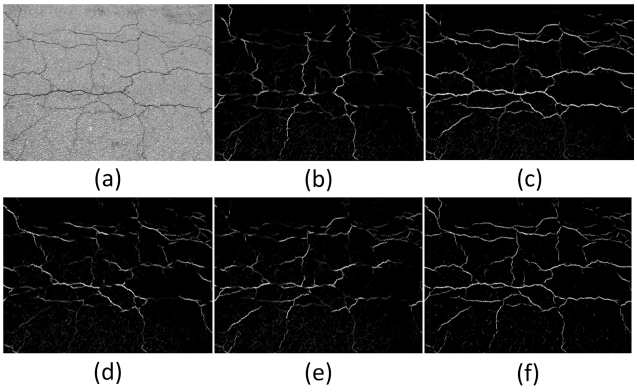

FIGURE 3. Process results of the proposed path anisotropy measurement under scale $l = 30$. (a) Initial images, (b) result of $A^{o_1}_l$, (c) $A^{o_2}_l$ (d) $A^{o_3}_l$, (e) $A^{o_4}_l$, and (f) PA^*_l.

Fig. 3 illustrates the effect of the proposed path anisotropy measurement under a fixed scale. To fulfill the requirements of multi-scale measurement, the path length parameter l is

varied from l_{min} to l_{max} with a step l_{step}, and the proposed PCmPA measurement is calculated as:

$$PA^*(x,y) = \max_{l_{min}<l<l_{max}} \left\{ PA_l^*(x,y) \right\} . \quad (7)$$

The implementation process of the PCmPA algorithm is presented in Algorithm 1. To demonstrate the robustness of the PCmPA algorithm, a qualitative comparison with a path morphology based method- RORPO [18] is provided in Fig. 4, in which it is confirmed that PCmPA can effectively enhance crack structures.

Algorithm 1: PCmPA Algorithm

Input: Multi-orientational phase congruency maps $\{PC_{\theta_i} :|\ i = 1 \sim 12\}$, set of scales $l \in [l_{min}, l_{max}]$, set of orientations $O = \{o_1, o_2, o_3, o_4\}$

Output: Anisotropy measurement map PA^*

REM *Step1: local convolution enhancement*

for *each phase congruency map* PC_{θ_i} **do**

  $PC^*_{\theta_i} = PC_{\theta_i} * G_{\theta_i}$

end

$I_{PC}^{max} = \max_{\theta_i} \left\{ PC^*_{\theta_i} \right\}$;

REM *Step2: path anisotropy measurement*

for *each scale* $l \in [l_{min}, l_{max}]$ **do**

  for *each* o_j *in* O **do**

    compute four-orientational path opening $A_l^{o_j} = po\left\{ I_{PC}^{max} \right\}$

  end

  compute path anisotropy measurement PA_l^* *using Eq.*(5), *Eq.*(6)

end

REM *Step3: compute multi-scale path anisotropy measurement* PA^* *using Eq.*(7)

return PA^*

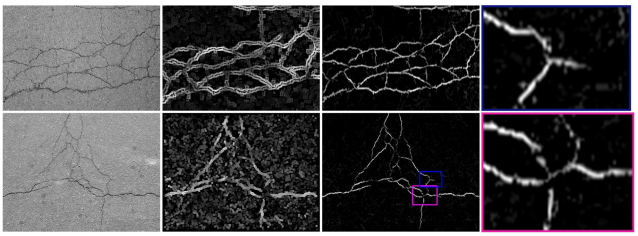

FIGURE 4. Comparison of the proposed algorithm for crack enhancement. (a) Initial images, (b) enhanced results by the RORPO [18] and (c) PCmPA algorithm, respectively, under the same parameters ($l_{min} = 30$, $l_{max} = 80$, and $l_{step} = 10$), and (d) enhanced results in selected regions with excessive bending or bifurcation.

C. MULTI-SCALE FREE-FORM ANISOTROPY MEASUREMENT

Despite improving the contrast of curvilinear structures and suppressing isotropic structures, one drawback exists when using the PCmPA algorithm. As phase congruency amplitudes at the intersection of cracks are low, this may result in lower responses derived from path operations (Fig. 4(d) illustrates this phenomenon). In this subsection, phase congruency based multi-scale free-form anisotropy filtering (PCmFFA) is proposed as an additional multi-scale anisotropy measurement to complement the PCmPA algorithm.

Free-form anisotropy (FFA) [34] measurement is a minimal path searching based pavement crack detection approach which relies on the assumption that minimal paths along cracks and backgrounds exhibit different statistical properties. As shown in Fig. 5, for a given pixel location x and a fixed searching radius d, four constrained minimal paths traversing x in different global orientations j (such as up-down, left-right, upper left-lower right, and upper right-lower left) are determined using the Dijkstra algorithm. The mean μ_j and variance σ_j of pixel radiometric values along these four minimal cost paths are the source for the measurement of coherence using sup-min function, and the free-form anisotropy is calculated as follows:

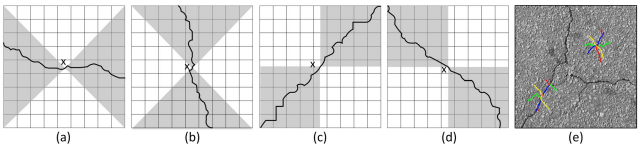

FIGURE 5. Minimal paths search strategy of FFA algorithm. (a)~(d) four-directional minimal paths search templates, (e) minimal paths pass through a crack pixel and a non-crack pixel.

$$FFA(x,y) = \frac{\max_j \left\{ h(\pi_j, \pi_{bgd}) \right\} - \min_j \left\{ h(\pi_j, \pi_{bgd}) \right\}}{\max_j \left\{ h(\pi_j, \pi_{bgd}) \right\}} , \quad (8)$$

where, $\pi_j = (\mu_j, \sigma_j)$ is the computed feature vector of minimal cost path along searched orientation j, $\pi_{bgd} = (\mu, \sigma)$ is the feature vector composed of intensity mean μ and standard deviation σ calculated on the whole image, and $h(\pi_j, \pi_{bgd}) = sup\left\{ min(\pi_j, \pi_{bgd}) \right\}$ is the evaluated degree of coherence between two sources calculated by sup-min function.

Although the original FFA algorithm has achieved good results, it contains three drawbacks:(1) It is difficult to adaptively detect cracks of different widths as the minimal path searching radius d is fixed; (2) As the feature vector π_{bgd} of the background region is estimated based on the whole image, its response value can be significantly affected by illumination and the non-uniform intensity; (3) For cracks with low contrast, the FFA response value is low, making it difficult to distinguish in subsequent processing.

To overcome the above obstacles, the PCmFA is proposed according to the following strategies. Firstly, the local coherence measurement is generalized by varying the searching radius d within $[d_{min}, d_{max}]$ with a step d_{step}, as shown in Fig. 6. The background cues are then estimated locally by each $(2*d+1)*(2*d+1)$ sized sub-image rather than the

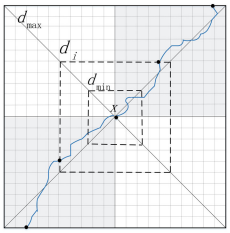

FIGURE 6. An illustration of minimal paths search strategy (along upper right-lower left orientation) of the PCmFFA algorithm.

whole image. Thus, the improved multi-scale FFA response at each pixel is defined as:

$$FFA^*(x,y) = \frac{1}{N_d}\sum_d \frac{1}{d}\cdot FFA_d(x,y)\,, \tag{9}$$

$$FFA_d(x,y) = \frac{\max\limits_j\left\{h(\pi_j^d,\pi_{bgd}^d)\right\} - \min\limits_j\left\{h(\pi_j^d,\pi_{bgd}^d)\right\}}{\max\limits_j\left\{h(\pi_j^d,\pi_{bgd}^d)\right\}} \tag{10}$$

where N_d is the number of scales and FFA_d is the anisotropy measurement at scale d. It should be noted that the combined multi-scale FFA response is a weighted linear combination on a per-pixel basis, which can emphasize the unequal contributions of different scales.

Algorithm 2: PCmFFA Algorithm

Input: Maximum phase congruency map I_{PC}^{max}, search radius $d \in [d_{min}, d_{max}]$
Output: Anisotropy measurement map FFA^*
$BW \leftarrow$ *binarized* I_{PC}^{max};
$ROI \leftarrow$ *obtain candidate crack regions from image BW;*
for *each pixel position* $(x,y) \in ROI$ **do**
  for *each scale* $d \in [d_{min}, d_{max}]$ **do**
    $\pi_{bgd}^d \leftarrow$ *the distribution of* $(2*d+1)*(2*d+1)$ *window around* (x,y);
    $P_j^d \leftarrow$ *search four-directional minimal paths* $(j = 1,2,3,4)$;
    $\pi_j^d \leftarrow$ *compute the distribution of each path* P_j^d;
    compute $FFA_d(x,y)$ *using Eq.*(10);
  end
  compute $FFA^*(x,y)$ *using Eq.*(9);
end
return FFA^*

To guarantee uniform responses, the generalized multi-scale FFA algorithm is focused on the maximum phase congruency map I_{PC}^{max}, rather than the raw pavement image. Finally, to improve computational efficiency, points with low phase congruency amplitude and isolated small regions derived from the binarized phase congruency map are discarded and not passed to the PCmFFA filter, as it is generally impossible that they will belong to crack structures. The implementation process of the presented PCmFFA algorithm is summarized in Algorithm 2.

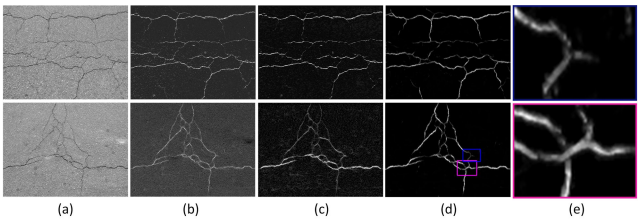

FIGURE 7. Comparison of the PCmFFA algorithm for crack enhancement. (a) Initial images, (b) images enhanced by FFA algorithm with fixed parameter $d = 30$, (c) and (d) images enhanced by the proposed multi-scale FFA algorithm and PCmFFA, respectively, under the same parameters ($d \in [20, 50]$ with a step $d_{step} = 5$), and (e) enhanced results in selected regions.

To verify the effectiveness, the enhanced results of the PCmFFA algorithm and original FFA algorithm are illustrated in Fig. 7. It can be observed that PCmFFA provides a significant improvement both in the suppression of texture noise and maintaining the local uniformity. More importantly, the PCmFFA algorithm can obtain uniform enhancement effects at bifurcations, which compensates for the shortcomings of the PCmPA algorithm. However, for excessively curved structures, the four-direction minimal path searching templates prescribed by the PCmFFA may not match the extension direction of real cracks, resulting in lower responses. Fortunately, the PCmPA filter is not subject to this constraint.

D. CRACKS SEGMENTATION USING OPTIMIZED SEGMENTATION MODEL

The above two proposed multi-scale curvilinear structure filters are complementary to each other and provide reliable geometric measurements of crack and non-crack. Higher detection accuracy can thus be expected when combining information from both. In this work, an optimized segmentation technique based on a novel graph-cuts model is presented for crack pixel classification.

Segmenting tasks using graph-cuts technique [42] can be treated as finding an optimal labeling $f : I_p \rightarrow L$, which assigns a label $L_p \in L$ to each pixel $p \in I$. In this work, the set of labels L is defined as $L = \{0, 1\}$, in which 1 indicates crack pixels and 0 refers to background pixels. By combining appearance feature and geometric priors (crack probability map defined by PCmPA and PCmFFA), the energy function for the graph-cuts minimization is defined as:

$$E(L) = \sum_{p\in I}(\omega_1\mathcal{D}_p(L_p) + \omega_2\mathcal{D}_p^{PCmPA}(L_p) + \omega_3\mathcal{D}_p^{PCmFFA}(L_p)) + \lambda\sum_{\{p,q\}\in\mathcal{N}}\mathcal{V}_{\{p,q\}}(L_p,L_q)\,, \tag{11}$$

where the data term consists of appearance feature $\mathcal{D}_p(\cdot)$ and two geometric features, $\mathcal{D}_p^{PCmPA}(\cdot)$ and $\mathcal{D}_p^{PCmFFA}(\cdot)$, and ω_1, ω_2, and ω_3 are weight parameters balancing these three components. The smoothness term $\mathcal{V}_{\{p,q\}}(L_p, L_q)$ provides a measure for cutting the edge (p, q), $\mathcal{N}$ is the set of

8-neighboring pixels, and λ is a weighted parameter for adjusting the smoothness.

Energy data term: In Eq.(11), the data term $\mathcal{D}_p(L_p)$ defines the individual penalty for classifying each pixel to object or background according to intensity information. To avoid interference from uneven intensity, I_{PC}^{max} is used as the appearance feature, and the penalty can be captured by the likelihood determined by the estimation of intensity distribution for cracks and background pixels as:

$$\mathcal{D}_p(L_p|L_p = L) = e^{-\frac{(I_{PC}^{max} - m_L)^2}{2\delta_L^2}}. \quad (12)$$

Similarly, the data terms $\mathcal{D}_p^{PCmPA}(L_p)$ and $\mathcal{D}_p^{PCmFFA}(L_p)$ can be determined by estimating the probability distribution of the foreground and background according to the following formula:

$$\mathcal{D}_p^{PCmPA}(L_p|L_p = L) = e^{-\frac{(PA^* - m_L^{PA^*})^2}{2(\delta_L^{PA^*})^2}}, \quad (13)$$

$$\mathcal{D}_p^{PCmFFA}(L_p|L_p = L) = e^{-\frac{(FFA^* - m_L^{FFA^*})^2}{2(\delta_L^{FFA^*})^2}}. \quad (14)$$

For the estimation of free parameters (m_L, δ_L), $(m_L^{PA^*}, \delta_L^{PA^*})$ and $(m_L^{FFA^*}, \delta_L^{FFA^*})$ in Eq.(12) $\sim$ (14), each corresponding global binarized map is taken as an initialized foreground region. The Gaussian probability distributions of foreground/background regions that build on the appearance and geometric prior terms can thus be estimated by fitting their mean value and standard deviation.

Energy smoothness term: The smoothness term provides a measure of discontinuity between two neighboring pixels $p, q \in I$ with labels $L_p, L_q \in L$. Let $I_{PC_p}^{max}$ and $I_{PC_q}^{max}$ be the intensity values of neighbor pixels p and q, respectively. A measure of smoothness is then defined as:

$$\mathcal{V}_{\{p,q\}}(L_p, L_q) = \delta(L_p, L_q) \cdot e^{-\frac{(I_{PC_p}^{max} - I_{PC_q}^{max})^2}{2\sigma^2}} \cdot \frac{1}{\|p - q\|} \quad (15)$$

where $\delta(L_p, L_q)$ is the metric to measure the cost of labeling smoothness between the labels L_p and L_p. If L_p and L_q have different labels, it is denoted as $\delta(L_p, L_q) = 1$, otherwise, it is defined as 0. σ controls the smoothness uncertainty.

Adaptive regularization parameter: In general graph-cuts algorithms, the data term and smoothness term are balanced by a fixed regularization parameter over the entire image, which may lead to under or over-segmentation results for some regions. It is also difficult to independently determine the most suitable regularization parameter for different application scenarios using this approach. In the crack segmentation task, smaller λ are expected at the boundaries between cracks and backgrounds to encourage their elimination. Inside backgrounds and crack structures, a higher λ is required to maintain the overall continuity of detected structures. Based on this, an adaptive regularization parameter λ^* is introduced here for a local adaptive balancing effect.

For each pixel p pixels in I_{PC}^{max}, the average phased congruency of pixels with a magnitude larger than threshold t in the ε-neighborhood of p is first determined and defined as:

$$\gamma = \sum_{i \in \mathcal{N}_\varepsilon} I_{PC_i}^{max}(I_{PC_i}^{max} \geq t) / \sum_{i \in \mathcal{N}_\varepsilon} (I_{PC_i}^{max} \geq t), \quad (16)$$

where $\mathcal{N}_\varepsilon = \{i \mid \|i - p\| \leq \varepsilon, i \in I_{PC}^{max}, p \in I_{PC}^{max}\}$. The resulting image γ can be regarded as a significance measure of the phase consistency amplitude in a local range. In the experiments, ε is set as 5-pixels, and a suitable t can be estimated through the corresponding phase congruency distribution (such as the mean μ_{PC} and variance σ_{PC}) in foreground regions obtained by adaptive binarized PCmPA and PCmFFA response maps. According to the authors' experience, $t = \mu_{PC} - \sigma_{PC}$ is suitable.

The weighted Laplace operator on the normalized γ is then employed to obtain the edge map $\psi_{p,q}$ which is expressed as:

$$\begin{aligned}\psi_{p,q} = \frac{1}{12}\{&|\gamma_{p-1,q+1} - \gamma_{p,q}| + 2|\gamma_{p,q-1} - \gamma_{p,q}| \\ &+ |\gamma_{p+1,q-1} - \gamma_{p,q}| + 2|\gamma_{p-1,q} - \gamma_{p,q}| \\ &+ |\gamma_{p-1,q-1} - \gamma_{p,q}| + 2|\gamma_{p+1,q} - \gamma_{p,q}| \\ &+ |\gamma_{p+1,q+1} - \gamma_{p,q}| + 2|\gamma_{p,j+1} - \gamma_{p,q}|\}. \end{aligned} \quad (17)$$

Finally, $\psi_{p,q}$ is normalized to [0, 1] and the adaptive regularization parameter of each pixel is defined as:

$$\lambda_{p,q}^* = \alpha \cdot (1 - \psi_{p,q}), \quad (18)$$

where α is used to control the highest levels of smoothing and it is fixed as $\alpha = 0.25$ in the experiments.

Fig. 8 provides a qualitative comparison of the edge-filtering algorithm [43] for computing the adaptive regularization parameter. It can be seen that the presented method can capture the boundaries with a good filtering effect on the edges of non-curvilinear structures.

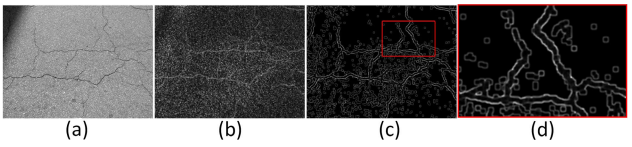

FIGURE 8. The edge maps of adaptive regularization parameter methods.(a) Initial image, (b) result of edge-filtering [42], (c) result of the proposed algorithm, and (d) zoom-in on selected region.

Weights assigning: The computational model of optimized segmentation is presented in Eq.(11), however, how the data terms are combined must still be determined. To solve this problem, $\mathcal{D}_p$, $\mathcal{D}_p^{PCmPA}$, and $\mathcal{D}_p^{PCmFFA}$ are separately used as data term focus on the computational model to obtain three different classifiers, then the weights are assigned according to the F1-measure obtained on a training dataset by different classifiers. That is, the weight ω_k associated with classifiers k can be calculated as:

$$\omega_k = \frac{F1_k}{\sum_{k=1}^{3} F1_k}, \quad (19)$$

where $\omega_k \in [0, 1]$, $\sum_{k=1}^{3} \omega_k = 1$, and $F1_k$ is the average F1-measure obtained by classifiers k. It is obvious that the weights are proportional to the corresponding F1-measure values.

After obtaining the final segmentation results with the proposed model, some grain-like false cracks may also be included. The elimination method [44] is then used to remove crack paths with a length shorter than 20-pixels.

IV. EXPERIMENTAL RESULTS AND ANALYSIS

Pavement image datasets, evaluation metrics, and baseline approaches are first introduced in this section. Parameter setting is then analyzed, and a series of comparative experiments are carried out to evaluate the proposed algorithm. The algorithm is implemented in MATLAB on an Intel Core i5 processor clocked at 2.50 GHz with 8G RAM, and demos of the PCmPA and PCmFFA algorithm are made available at GitHub repository: https://github.com/DrEdwardLee/PCmPA-PCmFFA.

A. DATASETS, COUNTERPARTS, AND EVALUATION METRICS

Three datasets detailed below were tested in the experiments.

•*CFD* [2] This dataset is composed of 118 road pavement images taken by an iPhone 5 with the size 480 × 320 pixels, which can generally represent urban road surface conditions in Beijing, China. All images accompanied by manually labeled pixel-wise ground truth contours, and the crack width ranges from 1 to 3 mm. Images in this dataset contain noises such as shadows, oil spots, and water stains.

•*CrackTree260* [3] It contains 260 pavement images captured by an area-array camera under visible-light illumination. It reflects different types of pavement cracks (longitudinal, transverse, alligatoring) under changeable texture, and many of them suffer from degradation problems including shadows, occlusions, low contrast, and partially deteriorated white painting. Each ground truth is 1-pixel width crack centerline manually annotated by a specialized labeling tool.

•*LaserCrack* This self-captured dataset contains 60 point cloud images captured by the authors' laser crack measurement system that utilize 3D laser-imaging techniques to model pavement surface. The horizontal, vertical, and depth resolutions of the collected 3D points are 1mm, 10mm and 1mm, respectively. Before crack detection, the 3D road profiling data are transformed into 2D depth images with the size 1200 × 1500 pixels by a series of preprocessing.

To validate the performance of different crack detection algorithms, three commonly used pixel-level metrics, Precision (Pr), Recall (Re), and F1-measure (F), are considered in the evaluation protocol. The metrics are defined as:

$$Pr = \frac{TP}{TP+FP}, Re = \frac{TP}{TP+FN}, F = \frac{2 \cdot Pr \cdot Re}{Pr+Re}, \quad (20)$$

where TP, FP, and FN are the number of true positives, false positives, and false negatives, respectively.

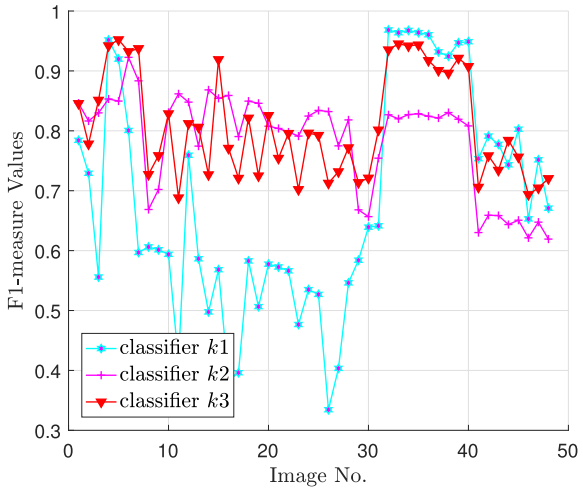

FIGURE 9. Crack segmentaion results with different classifier k (i.e. classifier $k1$ means the optimized segmentation model under weights combination $\{\omega_1 = 1, \omega_2 = 0, \omega_3 = 0\}$).

Six state-of-the-art pavement crack detection algorithms are selected for comparison, including the pattern classification based method CrackIT [44], two bio-inspired filtering-based methods, B-COSFIRE [29] and RUSTICO [30], two minimal path searching based methods, FFA [34] and MFCD [45], and the deep learning based network DeepCrack [3].

According to the related works [3], [30], a certain tolerance between the detected crack and the ground-truth is allowed for the performance evaluation. Specifically, if a detected pixel is not farther than d^* pixels from the nearest ground truth pixel, it is considered as a true positive, otherwise it is a false positive. In all comparisons, the tolerance distance d^* is set as 5 pixels. Besides, for the filter response results of both B-COSFIRE and RUSTICO, non-maximum suppression and hysteresis thresholding techniques are employed to obtain the thinned and binarized map under optimal parameters as recommended by their authors. In addition, for the results generated by DeepCrack, which are thin crack maps with the size of 512 × 512, size rescaling operators are applied to the maps to make them have the same size as the corresponding ground-truth.

B. PARAMETER SETTING

Parameters that must be determined in the proposed algorithm include three main categories: parameters for PCmPA filtering, parameters for PCmFFA filtering, and weighting parameters for the optimized segmentation model.

As the parameters involved in the PCmPA and PCmFFA filtering algorithms are related to the geometric characteristics of cracks (i.e. minimum length and width of cracks), considering the resolution of three datasets, parameters for PCmPA filtering are set as $l_{min} = 20$, $l_{step} = 10$, $l_{max} = 80$, and parameters for PCmPA filtering are fixed as $d_{min} = 20$, $d_{step} = 5$, $d_{max} = 50$. It should be noted that the removal of

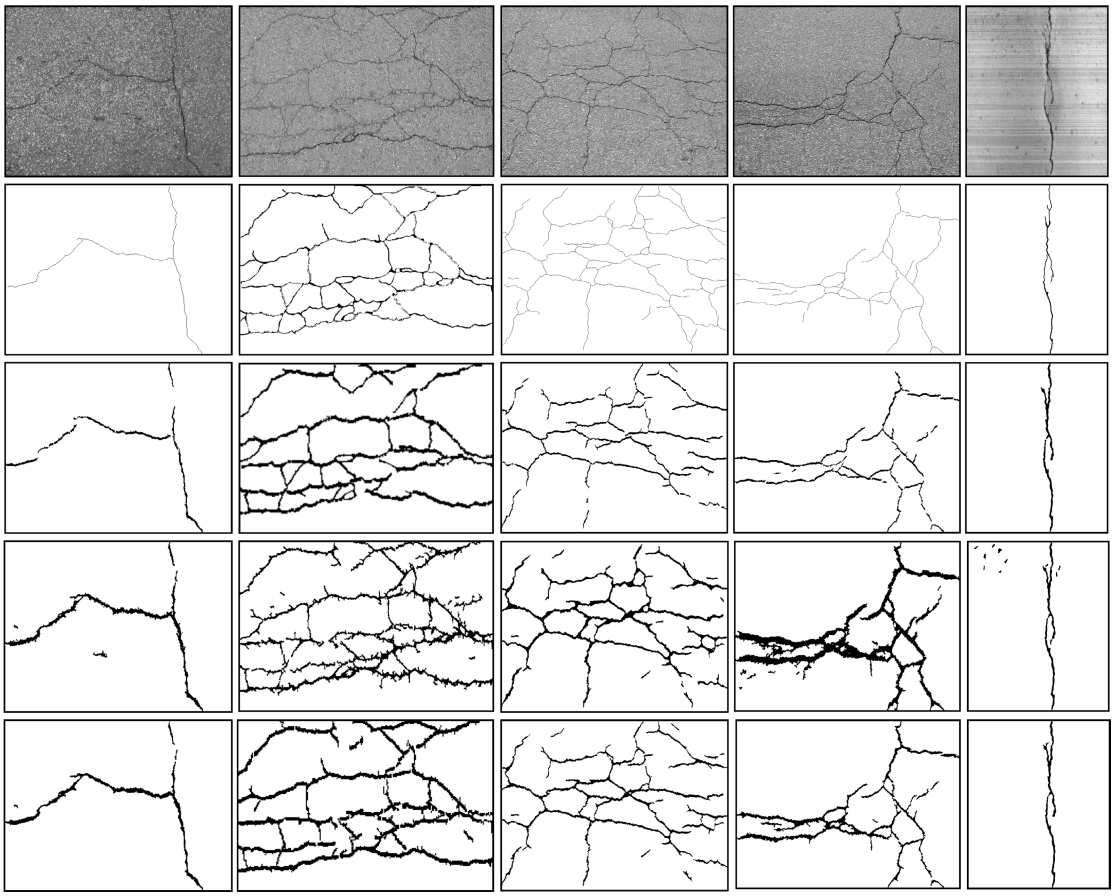

FIGURE 10. Crack segmentation results with different models (From top to bottom: original pavement images, ground truth, cracks detected by the model only with PCmPA priors, the model only with PCmFFA priors, and the proposed model).

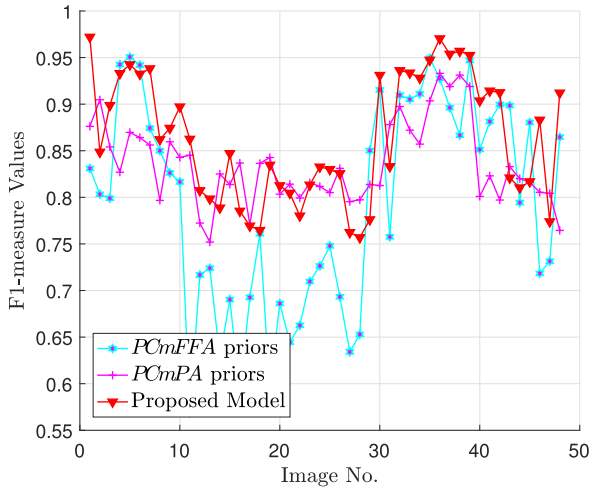

FIGURE 11. F1-measure value on the selected 48 images.

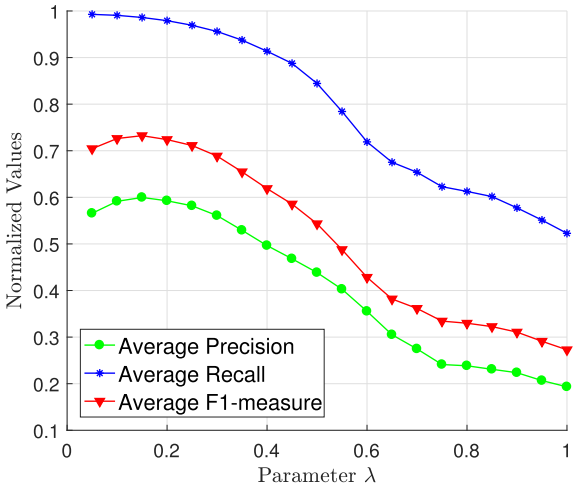

FIGURE 12. The obtained average Precision, average Recall, and average F1-measure value under different parameters λ.

unlikely crack pixels before PCmFFA filtering is governed by an adaptive binarization, and isolated short paths (less than 20 pixels) on the binarized phase congruency map are also discarded directly and not passed to PCmFFA filtering.

The weighting parameters ω_1, ω_2, and ω_3 are crucial for determining classification accuracy. In this experiment, 48 images are randomly selected from three datasets to investigate detection performance on the images under

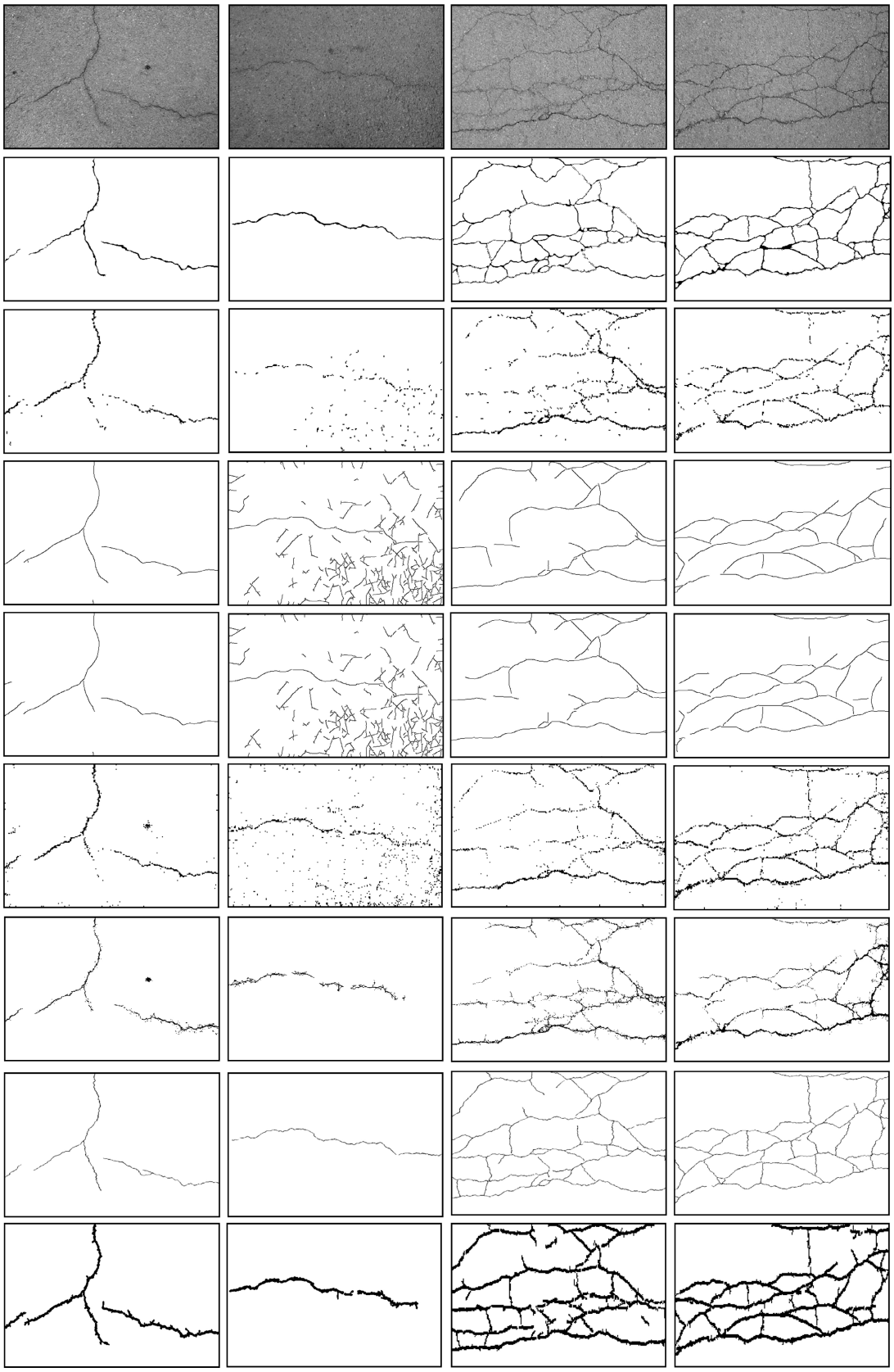

FIGURE 13. Crack detection results on four images selected from the CFD dataset set (From top to bottom: original pavement images, ground truth, cracks detected by CrackIT, B-COSFIRE, RUSTICO, FFA, MFCD, DeepCrack, and the proposed algorithm).

different classifiers. As shown in Fig. 9, the average F1-measure obtained by the three classifiers are 54.01%, 82.15%, 79.93%, respectively. After a simple calculation according to Eq.(19), it is clear that the combination of weights: $\omega_1 = 0.25$, $\omega_2 = 0.38$, and $\omega_3 = 0.37$ are suitable for the proposed optimized segmentation model.

C. VALIDATION OF THE PROPOSED MODEL

Before comparing with the state-of-the-art methods, we quantitatively analyze the effectiveness of the proposed model from two aspects, including (1) the necessity of combining two structure priors, PCmPA and PCmFFA; (2) the influence of the adaptive regularization parameter.

1) ABLATION STUDY

In this section, we evaluate the detection performance of models under different combinations of prior terms. Therefore, three models need to be compared, that is (1) model only with PCmPA priors (data term contains $\mathcal{D}_p$ and $\mathcal{D}_p^{PCmPA}$); (2) model only with PCmFFA priors (data term contains $\mathcal{D}_p$ and $\mathcal{D}_p^{PCmFFA}$); and (3) the proposed model (including both PCmPA priors and PCmFFA priors). Comparative experiments focused on the selected 48 test images under this three models are shown in Fig. 10, Fig. 11, and Table 1 respectively.

TABLE 1. Performance on the selected 48 images.

Model	Precision	Recall	F1-measure
PCmFFA priors	68.43%	**94.03%**	79.41%
PCmPA priors	78.89%	86.39%	83.58%
proposed model	79.92%	91.34%	**86.34%**

From the visual results in Fig. 10, it can be seen that the model only with PCmPA priors suffers missed detections problems at cracks with large bendings or branches. The model only with PCmFFA priors can compensate for this problem, while it is more susceptible to texture interference than that only with PCmPA priors, which causes some false positives near the real cracks. In contrast, the proposed model can be compromised in terms of missed detection and false detection to achieve acceptable detection results. As shown in Fig. 11 and Table 1, although the proposed model may not guarantee the best detection performance on each tested image, the average F1-measure obtained by it is as high as 86.34%, which is about 2.8% and 6.9% higher than models that only with PCmPA and PCmFFA priors, respectively. Thus, these comparison results convincingly demonstrate the effectiveness of the proposed model.

2) ADAPTIVE REGULARIZATION PARAMETER VS. FIXED REGULARIZATION PARAMETER

In order to investigate the impact of the fixed regularization parameter on detection performance and to verify the validity of the proposed adaptive parameter-determining strategy, in this part, the selected 40 images were tested by the model with different constant λ. Please notice that since the adaptive parameter $\lambda^*_{p,q}$ takes a value in $[0, 1]$ for each pixel (p, q), here, we just consider the detection performance under λ that changes from 0.01 to 1 with an interval of 0.05.

According to Fig. 12, one can see that, a smaller λ tends to increase among the average Precision, average Recall and average F1-measure, while a larger λ decrease these metrics. Although a better overall performance can be obtained under a small λ (i.e. $\lambda = 0.15$), the resulted average F1-measure value is relatively lower than that obtained by the proposed model with adaptive regularization parameter (which with an average F1-measure as 86.34%). From the above results, it reveals that the adaptive parameter-determining strategy indeed effectively improves the detection performance.

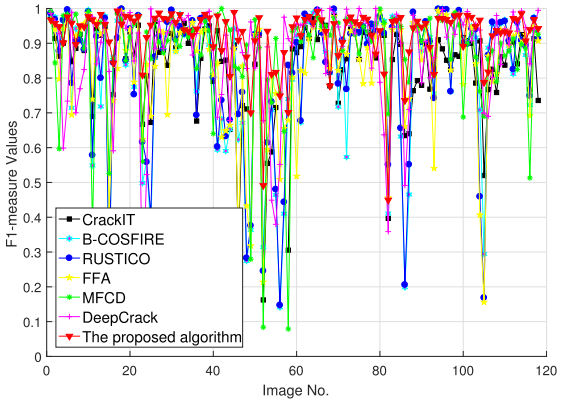

FIGURE 14. F1-measure value on the CFD dataset.

D. EVALUATIONS AND COMPARISONS

1) RESULTS ON CFD DATASET

Comparative experiments are first conducted on the CFD dataset, of which four images are randomly selected for qualitative assessment, as shown in Fig. 13. The F1-Measure and the performance evaluation are provided in Fig. 14 and Table 2, respectively. Note that the detection results of the DeepCrack algorithm are obtained by running web demo, and the results of other algorithms are downloaded from publicly available datasets.[1]

TABLE 2. Crack detection overall performance on CFD dataset.

Method	Precision	Recall	F1-measure
CrackIT	68.25%	86.90%	74.28%
B-COSFIRE	72.95%	86.01%	77.85%
RUSTICO	73.29%	85.66%	78.18%
FFA	66.35%	**95.64%**	74.65%
MFCD	**88.68%**	88.70%	87.04%
DeepCrack	88.15%	93.01%	**89.39%**
our method	87.25%	93.42%	88.76%

As shown in Fig. 13, the CrackIT toolbox provides discontinuous crack segments and produces false detection in the vicinity of real cracks. As the algorithm relies solely

[1] Downloadable from http://telerobot.cs.tamu.edu/bridge/Datasets.html.

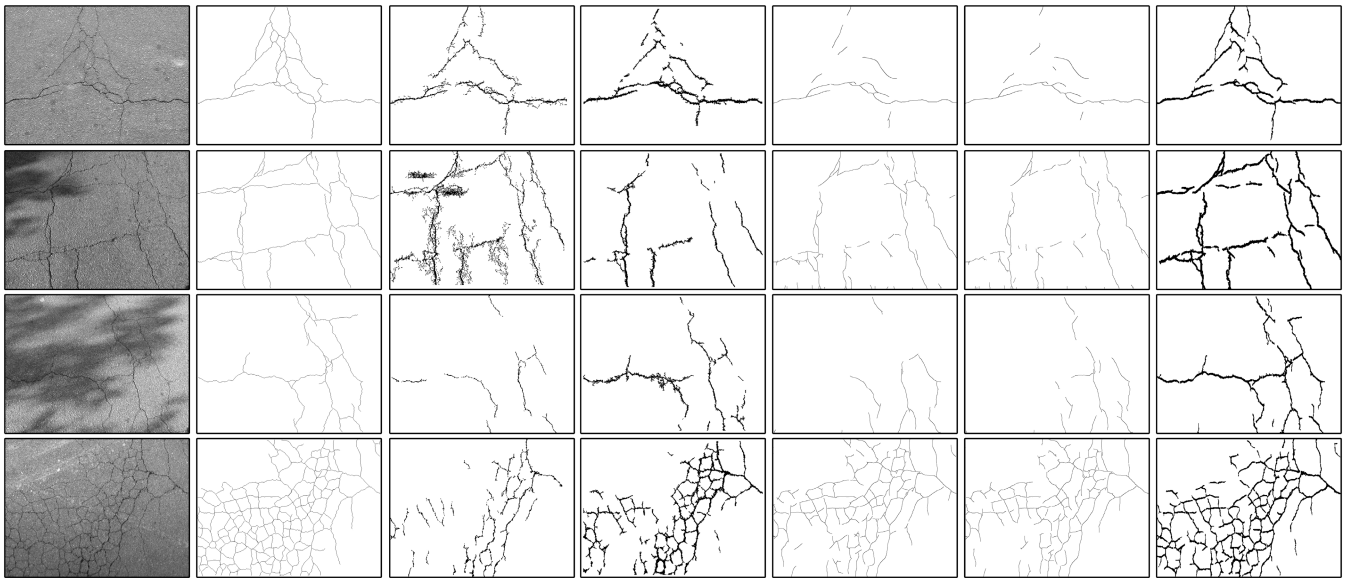

FIGURE 15. Crack detection results on the CrackTree260 dataset (From left to right: original pavement images, ground truth, cracks deteced by CrackIT, FFA, B-COSFIRE, RUSTICOFFA and the proposed algorithm).

on gray statistical cues (the mean and standard variation) of each small image block and does not consider the geometric properties of cracks, it is difficult to detect cracks with poor continuity and weak contrast. For cracks with good continuity and obvious contrast, both B-COSFIRE and RUSTICO can achieve desirable results. As the core concept of these two algorithms is based on Gabor filtering, when strong grain-like interference occurs on the road surface and the crack is ambiguous, the discrimination of the Gabor response for cracks and background area is poor, so that the detection performance of these two algorithms is degraded. As MFCD adopts a multi-scale fusion strategy in the stage of crack path selection and verification, its detection performance is better than FFA algorithm. However, for isotropic block-like targets, it lacks recognition ability, resulting in false detection (as shown in the first image of the seventh row in Fig. 13). The results indicate that the proposed method outperforms the techniques above as it not only produces less noise, but maintains the continuity of cracks. Although the high-level semantic information based DeepCrack model shows superior generalization ability and achieves better TP on this dataset, it fails to detect small cracks near dense cracks.

The quantitative evaluation results are illustrated in Fig. 14 and Table 2. Although the F1-measure of the proposed algorithm on this dataset is not the best, at about 0.63% lower than the highest performing DeepCrack algorithm, it performs much better than the traditional algorithms mentioned above. It should also be noted that for cracks with extremely low contrast and excessive interference, both DeepCrack and the proposed algorithm produce missed detections, resulting in a decline in detection performance. The detections on the 24th and 81st samples in Fig. 14 provide an illustration of this problem in that their F1-Measure value is much lower than that of other samples.

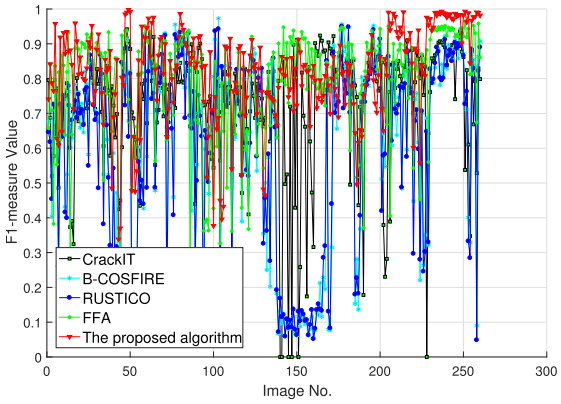

FIGURE 16. F1-measure value on the CrackTree260 dataset.

2) RESULTS ON CrackTree260 DATASET

Four publicly available algorithms including CrackIT, B-COSFIRE, RUSTICO, and FFA algorithms are selected as counterparts in this experiment to examine the effectiveness of the presented method. These algorithms are implemented using the source code or demos provided by the authors. Specifically, the detections of CrackIT algorithm are obtained under the optimal parameters selected in advance by multiple tests. The four-directional shortest path searching radius of FFA algorithms is set as $d = 30$ recommended by the author. For B-COSFIRE and RUSTICO, comparison experiments are conducted under fine-tuned parameters using a grid search strategy. As the DeepCrack model is trained on CrackTree260 dataset, it is not selected.

Fig. 15 shows the representative detections, where it can be observed that the performance of CrackIT is greatly affected by shadows. The recall rate of these four counterparts degrades when the contrast between crack and backgrounds

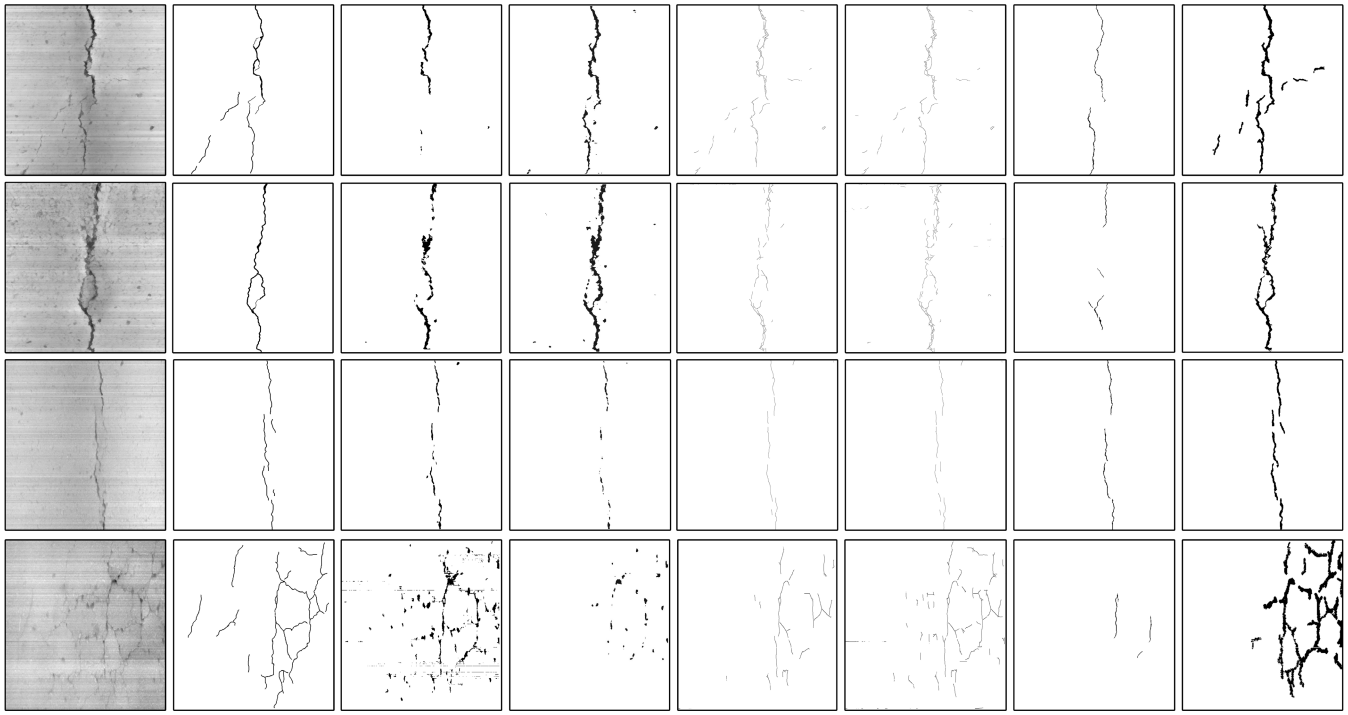

FIGURE 17. Crack detection results on the LaserCrack dataset (From left to right: original pavement images, ground truth, cracks deteced by CrackIT, FFA, B-COSFIRE, RUSTICOFFA, DeepCrack and the proposed algorithm).

is low. Although the proposed algorithm also delivers some missed detections, it is the most approximate to ground truth. The performance on the CrackTree260 dataset are summarized in Fig. 16 and Table 3, indicating that on this dataset, the proposed algorithm increases precision, recall, and F1-measure by 10.03%, 0.86%, and 7.69%, respectively, compared to the other algorithms.

TABLE 3. Crack detection overall performance on CrackTree260 dataset.

Method	Precision	Recall	F1-measure
CrackIT	69.02%	82.09%	72.14%
B-COSFIRE	65.70%	77.60%	70.93%
RUSTICO	64.94%	76.16%	69.22%
FFA	65.57%	90.48%	75.51%
our method	**79.05%**	**91.34%**	**83.20%**

Comparing Table 3 with Table 2, it can be seen that the performance of all algorithms on the CrackTree260 dataset is lower than that on the CFD dataset. This is mainly due to noise interference in the CrackTree260 dataset being more complicated than that of the CFD dataset.

3) RESULTS ON LaserCrack DATASET

The proposed algorithm is tested on the LaserCrack dataset and compared to the CrackIT, FFA, B-COSFIRE, RUSTICOFFA, and DeepCrack algorithms. Fig. 17 shows the qualitative detection results, where it can be observed that both CrackIT and FFA produce misdetection and result in a higher FP rate. For cracks with larger width or lower contrast, the DeepCrack algorithm shows obvious omission (as shown in the second and fourth images in the seventh column of Fig. 17).

TABLE 4. Crack detection overall performance on LaserCrack dataset.

Method	Precision	Recall	F1-measure
CrackIT	62.35%	78.00%	69.31%
B-COSFIRE	64.29%	73.31%	68.42%
RUSTICO	65.53%	72.91%	69.96%
FFA	60.80%	87.53%	71.58%
DeepCrack	**86.73%**	67.70%	73.63%
our method	76.92%	**89.44%**	**80.60%**

The overall performance of the comparison methods are listed in Table 4, which indicates that the proposed algorithm obtains the best result with an F1-measure value of 80.60%. Although DeepCrack achieves the best precision of 86.73% on this dataset, 9.81% higher than the proposed algorithm, it has a high false negative and results in an F1-measure that is 6.97% lower than the new algorithm. The reason for this phenomenon may be related to the characteristics of the LaserCrack dataset, which is significantly different to the CrackTree260 dataset that the DeepCrack network was trained on.

In terms of computational efficiency, the average running time on this dataset is listed in Table 5. As DeepCrack is based on GeForce GTX TITAN-X GPU, it is not suitable to compare. Besides, since the released demo of the FFA

TABLE 5. Comparison of computational time.

Method	CrackIT	B-COSFIRE	RUSTICO	our method
Time (s)	5.73	15.54	12.47	32.31

algorithm is an executable file, it is also not selected for comparison. Although the proposed algorithm takes more time than the CrackIT, B-COSFIRE and RUSTICO algorithms, considering the detection results, such running time is also tolerable.

As illustrated by the three experiments, the proposed algorithm is superior to low-level vision feature-based methods. In addition, the performance of all methods on the CrackTree260 and LaserCrack datasets are lower than that on the CFD dataset, which is related to the noise interference degree of these datasets. Although the performance of the proposed algorithm on CFD dataset is lower than DeepCrack, the new algorithm still exhibits obvious advantages as it does not require elaborately labeled training samples and has superior generalization capabilities.

V. CONCLUSION

An integrated system for the automatic delineation of pavement cracks was presented in this paper, in which crack pixels are extracted by solving an optimized segmentation framework merged crack geometric prior information. The two types of global curvilinear structure filtering methods PCmPA and PCmFFA were proposed to provide geometric prior features, and then integrated together with a crack appearance feature using a regularization parameter adaptive graph-cuts model. To the extent of the authors' knowledge, no previous work has combined global filtering technique and optimized segmentation model for the identification of cracks. Validation results on three pavement datasets demonstrated that the proposed algorithm is robust to uneven intensity and texture noise, and the overall performance obtained by the algorithm is superior to that of the comparison algorithms. Future research will be dedicated to investigating a reasonable fusion strategy that combines the deep learning model with the proposed hand-crafted geometric prior features to construct a more robust curvilinear structures detector.

REFERENCES

[1] L. Zhang, F. Yang, Y. Daniel Zhang, and Y. J. Zhu, "Road crack detection using deep convolutional neural network," in *Proc. IEEE Int. Conf. Image Process. (ICIP)*, Sep. 2016, pp. 3708–3712.

[2] Y. Shi, L. Cui, Z. Qi, F. Meng, and Z. Chen, "Automatic road crack detection using random structured forests," *IEEE Trans. Intell. Transp. Syst.*, vol. 17, no. 12, pp. 3434–3445, Dec. 2016.

[3] Q. Zou, Z. Zhang, Q. Li, X. Qi, Q. Wang, and S. Wang, "DeepCrack: Learning hierarchical convolutional features for crack detection," *IEEE Trans. Image Process.*, vol. 28, no. 3, pp. 1498–1512, Mar. 2019.

[4] F. Yang, L. Zhang, S. Yu, D. Prokhorov, X. Mei, and H. Ling, "Feature pyramid and hierarchical boosting network for pavement crack detection," *IEEE Trans. Intell. Transp. Syst.*, vol. 21, no. 4, pp. 1525–1535, Apr. 2020.

[5] C. L. Srinidhi, P. Aparna, and J. Rajan, "Recent advancements in retinal vessel segmentation," *J. Med. Syst.*, vol. 41, no. 4, p. 70, Apr. 2017.

[6] R. Alshehhi and P. R. Marpu, "Hierarchical graph-based segmentation for extracting road networks from high-resolution satellite images," *ISPRS J. Photogramm. Remote Sens.*, vol. 126, pp. 245–260, Apr. 2017.

[7] Z. Lv, Y. Jia, Q. Zhang, and Y. Chen, "An adaptive multifeature sparsity-based model for semiautomatic road extraction from high-resolution satellite images in urban areas," *IEEE Geosci. Remote Sens. Lett.*, vol. 14, no. 8, pp. 1238–1242, Aug. 2017.

[8] V. Bismuth, R. Vaillant, H. Talbot, and L. Najman, "Curvilinear structure enhancement with the polygonal path image-application to guide-wire segmentation in X-ray fluoroscopy," in *Proc. Int. Conf. Med. Image Comput. Comput.-Assist. Intervent.* Cham, Switzerland: Springer, 2012, pp. 9–16.

[9] G. Wang, C. Lopez-Molina, G. Vidal-Diez de Ulzurrun, and B. De Baets, "Noise-robust line detection using normalized and adaptive second-order anisotropic Gaussian kernels," *Signal Process.*, vol. 160, pp. 252–262, Jul. 2019.

[10] G. Sollazzo, K. C. P. Wang, G. Bosurgi, and J. Q. Li, "Hybrid procedure for automated detection of cracking with 3D pavement data," *J. Comput. Civil Eng.*, vol. 30, no. 6, Nov. 2016, Art. no. 04016032.

[11] C. Vicas and S. Nedevschi, "Detecting curvilinear features using structure tensors," *IEEE Trans. Image Process.*, vol. 24, no. 11, pp. 3874–3887, Nov. 2015.

[12] F. Denis, "Multidirectional curvilinear structures detection using steerable pyramid," *J. Electron. Imag.*, vol. 13, no. 4, pp. 756–766, Oct. 2004.

[13] S. Li, Y. Cao, and H. Cai, "Automatic pavement-crack detection and segmentation based on steerable matched filtering and an active contour model," *J. Comput. Civil Eng.*, vol. 31, no. 5, Sep. 2017, Art. no. 04017045.

[14] H. Chen, H. Zhao, D. Han, and K. Liu, "Accurate and robust crack detection using steerable evidence filtering in electroluminescence images of solar cells," *Opt. Lasers Eng.*, vol. 118, pp. 22–33, 2019.

[15] E. Zalama, J. Gómez-García-Bermejo, R. Medina, and J. Llamas, "Road crack detection using visual features extracted by Gabor filters," *Computer-Aided Civil Infrastructure Eng.*, vol. 29, no. 5, pp. 342–358, May 2014.

[16] T. Asplund and C. L. Luengo Hendriks, "A faster, unbiased path opening by upper skeletonization and weighted adjacency graphs," *IEEE Trans. Image Process.*, vol. 25, no. 12, pp. 5589–5600, Dec. 2016.

[17] P. Dokládal, "Statistical threshold selection for path openings to detect cracks," in *Proc. Int. Symp. Math. Morphology Appl. Signal Image Process.* Cham, Switzerland: Springer, 2017, pp. 369–380.

[18] O. Merveille, H. Talbot, L. Najman, and N. Passat, "Curvilinear structure analysis by ranking the orientation responses of path operators," *IEEE Trans. Pattern Anal. Mach. Intell.*, vol. 40, no. 2, pp. 304–317, Feb. 2018.

[19] Z. Qu, L. Bai, S.-Q. An, F.-R. Ju, and L. Liu, "Lining seam elimination algorithm and surface crack detection in concrete tunnel lining," *J. Electron. Imag.*, vol. 25, no. 6, Nov. 2016, Art. no. 063004.

[20] D. Ai, G. Jiang, L. Siew Kei, and C. Li, "Automatic pixel-level pavement crack detection using information of multi-scale neighborhoods," *IEEE Access*, vol. 6, pp. 24452–24463, 2018.

[21] Z. Liu, J. Wang, G. Liu, and L. Zhang, "Discriminative low-rank preserving projection for dimensionality reduction," *Appl. Soft Comput.*, vol. 85, Dec. 2019, Art. no. 105768.

[22] Z. Liu, Z. Lai, W. Ou, K. Zhang, and R. Zheng, "Structured optimal graph based sparse feature extraction for semi-supervised learning," *Signal Process.*, vol. 170, May 2020, Art. no. 107456.

[23] Y. Wu, B. Jiang, and N. Lu, "A descriptor system approach for estimation of incipient faults with application to high-speed railway traction devices," *IEEE Trans. Syst., Man, Cybern., Syst.*, vol. 49, no. 10, pp. 2108–2118, Oct. 2019.

[24] Y. Wu, B. Jiang, and Y. Wang, "Incipient winding fault detection and diagnosis for squirrel-cage induction motors equipped on CRH trains," *ISA Trans.*, 2019, doi: 10.1016/j.isatra.2019.09.020.

[25] L. Zhang, Q. Zhang, L. Zhang, D. Tao, X. Huang, and B. Du, "Ensemble manifold regularized sparse low-rank approximation for multiview feature embedding," *Pattern Recognit.*, vol. 48, no. 10, pp. 3102–3112, Oct. 2015.

[26] Z. Wang, B. Du, and Y. Guo, "Domain adaptation with neural embedding matching," *IEEE Trans. Neural Netw. Learn. Syst.*, early access, Sep. 13, 2019, doi: 10.1109/TNNLS.2019.2935608.

[27] F.-C. Chen and M. R. Jahanshahi, "NB-CNN: Deep learning-based crack detection using convolutional neural network and Naïve Bayes data fusion," *IEEE Trans. Ind. Electron.*, vol. 65, no. 5, pp. 4392–4400, May 2018.

[28] Z. Li, G. Xu, Y. Cheng, Z. Wang, and Q. Wu, "Graph network refining for pavement crack detection based on multiscale curvilinear structure filter," *J. Electron. Imag.*, vol. 28, no. 5, 2019, Art. no. 053035.
[29] N. Strisciuglio, G. Azzopardi, and N. Petkov, "Detection of curved lines with B-COSFIRE filters: A case study on crack delineation," in *Proc. Int. Conf. Comput. Anal. Images Patterns*. Cham, Switzerland: Springer, 2017, pp. 108–120.
[30] N. Strisciuglio, G. Azzopardi, and N. Petkov, "Robust inhibition-augmented operator for delineation of curvilinear structures," *IEEE Trans. Image Process.*, vol. 28, no. 12, pp. 5852–5866, Dec. 2019.
[31] L. Wu, S. Mokhtari, A. Nazef, B. Nam, and H.-B. Yun, "Improvement of crack-detection accuracy using a novel crack defragmentation technique in image-based road assessment," *J. Comput. Civil Eng.*, vol. 30, no. 1, Jan. 2016, Art. no. 04014118.
[32] H. Heijmans, M. Buckley, and H. Talbot, "Path openings and closings," *J. Math. Imag. Vis.*, vol. 22, nos. 2–3, pp. 107–119, May 2005.
[33] H. Talbot and B. Appleton, "Efficient complete and incomplete path openings and closings," *Image Vis. Comput.*, vol. 25, no. 4, pp. 416–425, Apr. 2007.
[34] T. S. Nguyen, S. Begot, F. Duculty, and M. Avila, "Free-form anisotropy: A new method for crack detection on pavement surface images," in *Proc. 18th IEEE Int. Conf. Image Process.*, Sep. 2011, pp. 1069–1072.
[35] Q. Li, Q. Zou, D. Zhang, and Q. Mao, "FoSA: F* seed-growing approach for crack-line detection from pavement images," *Image Vis. Comput.*, vol. 29, no. 12, pp. 861–872, Nov. 2011.
[36] R. Amhaz, S. Chambon, J. Idier, and V. Baltazart, "Automatic crack detection on two-dimensional pavement images: An algorithm based on minimal path selection," *IEEE Trans. Intell. Transp. Syst.*, vol. 17, no. 10, pp. 2718–2729, Oct. 2016.
[37] W. Kaddah, M. Elbouz, Y. Ouerhani, V. Baltazart, M. Desthieux, and A. Alfalou, "Optimized minimal path selection (OMPS) method for automatic and unsupervised crack segmentation within two-dimensional pavement images," *Vis. Comput.*, vol. 35, no. 9, pp. 1293–1309, Sep. 2019.
[38] P. Dollar and C. L. Zitnick, "Fast edge detection using structured forests," *IEEE Trans. Pattern Anal. Mach. Intell.*, vol. 37, no. 8, pp. 1558–1570, Aug. 2015.
[39] Y. LeCun, Y. Bengio, and G. Hinton, "Deep learning," *Nature*, vol. 521, no. 7553, pp. 436–444, 2015.
[40] P. Kovesi, "Image features from phase congruency," *J. Comput. Vis. Res.*, vol. 1, no. 3, pp. 1–26, 1999.
[41] L. Zhang, L. Zhang, D. Zhang, and Z. Guo, "Phase congruency induced local features for finger-knuckle-print recognition," *Pattern Recognit.*, vol. 45, no. 7, pp. 2522–2531, Jul. 2012.
[42] Y. Boykov, O. Veksler, and R. Zabih, "Fast approximate energy minimization via graph cuts," *IEEE Trans. Pattern Anal. Mach. Intell.*, vol. 23, no. 11, pp. 1222–1239, Nov. 2001.
[43] G. Cheng, Y. Wang, F. Zhu, and C. Pan, "Road extraction via adaptive graph cuts with multiple features," in *Proc. IEEE Int. Conf. Image Process. (ICIP)*, Sep. 2015, pp. 3962–3966.
[44] H. Oliveira and P. L. Correia, "CrackIT—An image processing toolbox for crack detection and characterization," in *Proc. IEEE Int. Conf. Image Process. (ICIP)*, Oct. 2014, pp. 798–802.
[45] H. Li, D. Song, Y. Liu, and B. Li, "Automatic pavement crack detection by multi-scale image fusion," *IEEE Trans. Intell. Transp. Syst.*, vol. 20, no. 6, pp. 2025–2036, Jun. 2019.

ZHENHUA LI received the B.S. degree in electrical engineering and automation, in 2012, and the M.S. degree in control engineering, in 2015. He is currently pursuing the Ph.D. degree in measurement techniques and measuring instruments with the Nanjing University of Aeronautics and Astronautics (NUAA), Nanjing, China. His research interests include computer vision, pattern recognition, and photoelectric measurement.

GUILI XU received the Ph.D. degree from Jiangsu University, in 2002. He is currently a Professor with the College of Automation Engineering, Nanjing University of Aeronautics and Astronautics (NUAA), Nanjing, China. He has authored over 100 publications. His current research interests are photoelectric measurement, computer vision, and intelligent systems.

YUEHUA CHENG received the Ph.D. degree from the Nanjing University of Aeronautics and Astronautics (NUAA), Nanjing, China, in 2012. She is currently an Associate Professor with the College of Automation Engineering, NUAA. Her current research interests are fault diagnosis and fault-tolerant control and lifespan prediction applied to the satellite attitude control systems.

ZHENGSHENG WANG received the Ph.D. degree in computational mathematics from the Nanjing University of Aeronautics and Astronautics (NUAA), Nanjing, China, in 2006. He is currently a Professor and the Associate Dean of the College of Science, NUAA. His research interests focus on numerical algebra and applications, matrix methods in data mining and pattern recognition, and computational methods in science and engineering.

QUAN WU received the B.S. degree in electrical engineering and automation, in 2013, and the M.S. degree in control engineering, in 2016. He is currently pursuing the Ph.D. degree with the Nanjing University of Aeronautics and Astronautics (NUAA), Nanjing, China. His research interests include machine vision, pattern recognition, and remote sensing technique.